

# Delayed leaf green-up is associated with fine particulate air pollution in China

Received: 11 September 2024

Accepted: 27 March 2025

Published online: 10 April 2025

 Check for updates

Wendi Qu<sup>1,2,9</sup>, Hao Hua<sup>1,2,9</sup>, Ting Yang<sup>3,9</sup>, Constantin M. Zohner<sup>4</sup>, Josep Peñuelas<sup>5,6</sup>, Jing Wei<sup>7</sup>, Le Yu<sup>8</sup>✉ & Chaoyang Wu<sup>1,2</sup>✉

Climate warming has led to earlier leaf green-up dates (GUD) with a greening trend of land surfaces in spring, yet the influence of multi-source particle pollution is not well understood. Using ground records and satellite observations of green-up date and fine particulate matter below 2.5  $\mu\text{m}$  ( $\text{PM}_{2.5}$ ) over the last two decades in China, here we show that  $\text{PM}_{2.5}$  pollution is associated with reduced plant carbon uptake and delayed green-up dates. These effects offset climate-driven spring greening and reduce subsequent photosynthesis in China. We find that pollution-associated delays in green-up date are primarily linked to increased chilling demands and higher heat requirements.  $\text{PM}_{2.5}$ -associated decreases in photosynthetically active radiation and maximum rate of carboxylation could also weaken plant photosynthetic capacity. Finally, when we incorporate a  $\text{PM}_{2.5}$  effect, phenological models predict up to a one-week delay in green-up date by the year 2060 compared to previous predictions. Negative feedbacks between anthropogenic pollution and terrestrial carbon uptake suggest unexpected uncertainty of China's carbon neutral targets resulting from air pollution, with far-reaching implications for both ecosystem health and policy-making.

With a 12% increase in global atmospheric  $\text{CO}_2$  concentration since 2000<sup>1</sup>, understanding the effects of climate change on photosynthetic processes is essential for comprehending and forecasting the upcoming carbon cycle. The carbon uptake of terrestrial ecosystems has increased due to elevated  $\text{CO}_2$  levels, climate warming<sup>2–4</sup>, land-use management practices<sup>5,6</sup>, and climate-driven advances in spring leaf green-up dates (GUD) across local, regional, and continental scales<sup>7–11</sup>. However, certain complex mechanisms, which are not yet fully comprehended, have the potential to negate the advanced GUD and enhanced plant photosynthesis, including factors like air pollution. This complexity presents considerable difficulties when attempting to predict the future potential of carbon uptake.

China has played a significant role in the global effort to conserve and restore forests, contributing to a greening of the terrestrial surface<sup>5</sup>. Together with natural greening processes due to climate change<sup>2,3</sup>, these initiatives have led to an increase in the carbon sink of China's terrestrial ecosystems, aiding in reducing atmospheric  $\text{CO}_2$  levels. However, China is also facing a major challenge with air pollution, particularly in its rapidly growing cities, where emissions of fine particulate matter ( $\text{PM}_{2.5}$ ) are of high record<sup>12</sup>. This pollution negatively impacts human health<sup>13–15</sup>, however, its effects on GUD and carbon uptake remain poorly understood.

Although the considerable influence of human activities on ecosystem functions is widely acknowledged<sup>16</sup>, the effects of  $\text{PM}_{2.5}$

<sup>1</sup>The Key Laboratory of Land Surface Pattern and Simulation, Institute of Geographical Sciences and Natural Resources Research, Chinese Academy of Sciences, Beijing, China. <sup>2</sup>University of the Chinese Academy of Sciences, Beijing, China. <sup>3</sup>State Key Laboratory of Atmospheric Boundary Layer Physics and Atmospheric Chemistry, Institute of Atmospheric Physics, Chinese Academy of Sciences, Beijing, China. <sup>4</sup>Department of Environmental Systems Science, Institute of Integrative Biology, ETH, Zurich, Zurich, Switzerland. <sup>5</sup>CSIC, Global Ecology Unit CREAM-CSIC-UAB, Barcelona, Catalonia, Spain. <sup>6</sup>CREAF, Barcelona, Catalonia, Spain. <sup>7</sup>Department of Atmospheric and Oceanic Science, Earth System Science Interdisciplinary Center, University of Maryland, College Park, MD, USA. <sup>8</sup>Department of Earth System Science, Ministry of Education Key Laboratory for Earth System Modeling, Institute for Global Change Studies, Tsinghua University, Beijing, China. <sup>9</sup>These authors contributed equally: Wendi Qu, Hao Hua, Ting Yang. ✉ e-mail: [leyu@tsinghua.edu.cn](mailto:leyu@tsinghua.edu.cn); [wucy@igsnr.ac.cn](mailto:wucy@igsnr.ac.cn)

pollution in China over the past 20 years on plant activity have not yet been determined. PM<sub>2.5</sub> pollution could change the transmission of visible light and substantially decrease atmospheric clarity<sup>17</sup>, potentially regulating spring vegetation growth by altering microclimate (temperature and radiation)<sup>18</sup> and plant activities (leaf gas exchange and photosynthesis)<sup>19–21</sup>. For example, particulate pollution on weekdays could inhibit satellite-detected photosynthesis by reducing light availability in Europe, suggesting the regulation of human activities on ecosystem carbon dynamics<sup>22</sup>. Aiming at a broader view of PM<sub>2.5</sub> pollution impacts on GUD and carbon uptake, we utilized satellite-driven PM<sub>2.5</sub> data records<sup>23</sup>, together with a ground monitoring network of GUD with 1030 site-species time series<sup>24</sup> (Supplementary Fig. 1), and satellite-derived GUD<sup>25</sup> and solar-induced fluorescence (SIF, a proxy of plant photosynthesis)<sup>26</sup> since the 2000s for terrestrial ecosystems in China (Supplementary Table 1). We investigated the responses of spring GUD and SIF to PM<sub>2.5</sub> pollution from site to regional scales. We also explored potential biogeochemical and biogeophysical mechanisms under the PM<sub>2.5</sub>-GUD relationship, considering the pollution-driven alterations in winter chilling accumulation (CA), heat requirement (HR), and photosynthetic rate. As a last step, we incorporated PM<sub>2.5</sub> pollution into phenological models and predicted future projections of spring GUD under different emission scenarios that are central to China's efforts to realize carbon-neutral targets.

## Results

### Earlier GUD is associated with alleviated PM<sub>2.5</sub> pollution

Through a comprehensive evaluation of GUD from both ground and satellite observations, we explored the impacts of PM<sub>2.5</sub> pollution and climate on GUD and SIF (Methods). We found highly consistent temporal patterns between variations of the anomaly of spring PM<sub>2.5</sub> (March–May) and ground GUD from 2003 to 2018 for each site and each species (site-species-independent time series,  $n = 1030$ ) (Fig. 1A). A further partial correlation analysis, excluding effects of temperature, precipitation, and radiation, showed that spring GUD delayed significantly with increased PM<sub>2.5</sub>. The proportions of significant positive (delaying effects) and negative (advancing effects) GUD-PM<sub>2.5</sub> correlations were 11.8% and 5.0, respectively ( $p < 0.05$ ) (Fig. 1B). Further analysis of sensitivity, using ridge regression to mitigate potential multicollinearity between PM<sub>2.5</sub> and climatic factors (Methods), revealed that the advancement of GUD due to spring temperature was significantly offset by PM<sub>2.5</sub> pollution. For example, ground GUD had a sensitivity of  $-0.47$  (advanced GUD, unitless) for temperature, but PM<sub>2.5</sub> delayed GUD with a sensitivity of  $0.11$  (unitless). Using satellite GUD provides similar results, only differing in the magnitudes. The sensitivities of GUD and SIF to PM<sub>2.5</sub> were much stronger than those to precipitation and radiation. Grouping PM<sub>2.5</sub> sensitivities into different plant species (Supplementary Fig. 2) and vegetation types (Supplementary Fig. 3) confirms the widespread adverse effects of PM<sub>2.5</sub> on spring vegetation activities. The spatial analysis of nine regions across China showed consistent impacts of PM<sub>2.5</sub> pollution on spring GUD and SIF (Fig. 1D–L). Specifically, higher PM<sub>2.5</sub> pollution consistently led to delays in GUD (Supplementary Fig. 4), especially for relatively dry and cold regions (Supplementary Fig. 5). These findings reveal that PM<sub>2.5</sub> pollution offsets the ongoing earlier trends in spring phenology in China.

### Potential mechanisms under PM<sub>2.5</sub>-GUD relationships

Mechanisms through both biogeophysical and biogeochemical paths may underlay the response of spring GUD to PM<sub>2.5</sub> pollution. First, we investigated the impacts of PM<sub>2.5</sub> pollution on the chilling accumulation (CA, the chilling demand for plants during endodormancy) and the heat requirement (HR, the accumulated forcing temperature required for a phenological event), simulated by 11 CA models and five HR models (see “Methods”). We found that higher PM<sub>2.5</sub> caused a significant increase in CA after removing the effects of temperature

variations during CA periods (Fig. 2A). Because CA and GUD were also positively correlated, increased PM<sub>2.5</sub> led to delayed GUD. In addition, higher PM<sub>2.5</sub> also slightly increased HR, as evidenced by positive partial correlations between PM<sub>2.5</sub> and HR, after excluding the effects of preceding CA and temperature variations during HR periods. PM<sub>2.5</sub>-induced increases in HR contributed to a later GUD accordingly, with strong and positive partial correlations between HR and GUD (Fig. 2B). Analyses on ground GUD were consistent for these correlations (Fig. 2C). Biogeochemically, an increase in PM<sub>2.5</sub> significantly decreased the maximum rate of carboxylation ( $V_{C_{max}}$ ), an indicator of leaf photosynthetic capacity, with 26.9% (out of 84.4%) negative correlations compared with only 0.7% (out of 15.6%) of positive correlations ( $p < 0.05$ ) (Fig. 2D). Since  $V_{C_{max}}$  positively correlated with SIF, higher PM<sub>2.5</sub> negated spring plant growth consequently (Fig. 2E). A negative correlation between PM<sub>2.5</sub> pollution and photosynthetically active radiation (PAR) confirmed the PM<sub>2.5</sub>-induced decreases in light availability (Fig. 2F). Lower PAR greatly reduced the rate of photosynthesis, declining the potential of spring greening under climate change. PM<sub>2.5</sub>-induced increase in diffuse PAR was limited, showing minor effects on plant productivity (Supplementary Fig. 6). Structural equation modeling (SEM) generally supported our hypothesis that PM<sub>2.5</sub> increased chilling accumulation, decreased  $V_{C_{max}}$ , and delayed GUD accordingly, further regulating spring SIF (Fig. 2G).

### GUD model improvements and future projections

We developed a series of new spring GUD models by incorporating the effects of PM<sub>2.5</sub> using several algorithms, including one-phase algorithms (growing degree days and spring warming) and two-phase algorithms (sequential model and parallel model). Our findings revealed that models incorporating PM<sub>2.5</sub> resulted in significantly better estimates of GUD, as evidenced by the higher percentages of pixels with significant correlations between model estimates and satellite observations, a higher average correlation coefficient ( $R$ ), a lower average root mean square error, and a higher Kling-Gupta efficiency (Fig. 3). Besides, two-phase (chilling and forcing) algorithms showed better performances when PM<sub>2.5</sub> adjusted both phases. Using ground GUD, we confirmed the improvement of GUD models by incorporating PM<sub>2.5</sub> effects (Supplementary Fig. 7).

Among these GUD models, the sequential model incorporating PM<sub>2.5</sub> effects into chilling and forcing phases performed the best in modeling GUD with the lowest RMSE and highest KGE. Hence, we employed this model to predict GUD for China and compared its estimates with current temperature-driven sequential model under three future emission scenarios based on the Dynamic Projection Model for Emissions in China (DPEC v1.1): a best-health-effect scenario (SSP1-Neutrality-BHE), an enhanced-control-policy scenario (SSP2-45-ECP), and a business-as-usual scenario (SSP4-60-BAU) (Methods, Fig. 4). The difference in GUDs modeled with and without accounting for PM<sub>2.5</sub> using the sequential model was more pronounced in scenarios predicting higher pollution levels. Notably, the greatest GUD difference occurred under the high-emission SSP4 scenario. However, this difference is expected to decrease over time, as PM<sub>2.5</sub> pollution is projected to decline across all scenarios. We also tested for spatial differences in GUD projections with different levels of PM<sub>2.5</sub> and found that GUD was typically more delayed in areas with high PM<sub>2.5</sub> pollution, such as northern China and central China, especially under the high-emission scenario (Fig. 4B, C). The one-phase GUD model (i.e., spring warming) projections also supported these results for all emission scenarios (Supplementary Fig. 8).

## Discussion

Using multiple ground and satellite observations, we found that ambient PM<sub>2.5</sub> pollution in China has reduced carbon uptake mainly by offsetting climate-induced earlier GUD. These results enhance our understanding of how human activities, including economic and social

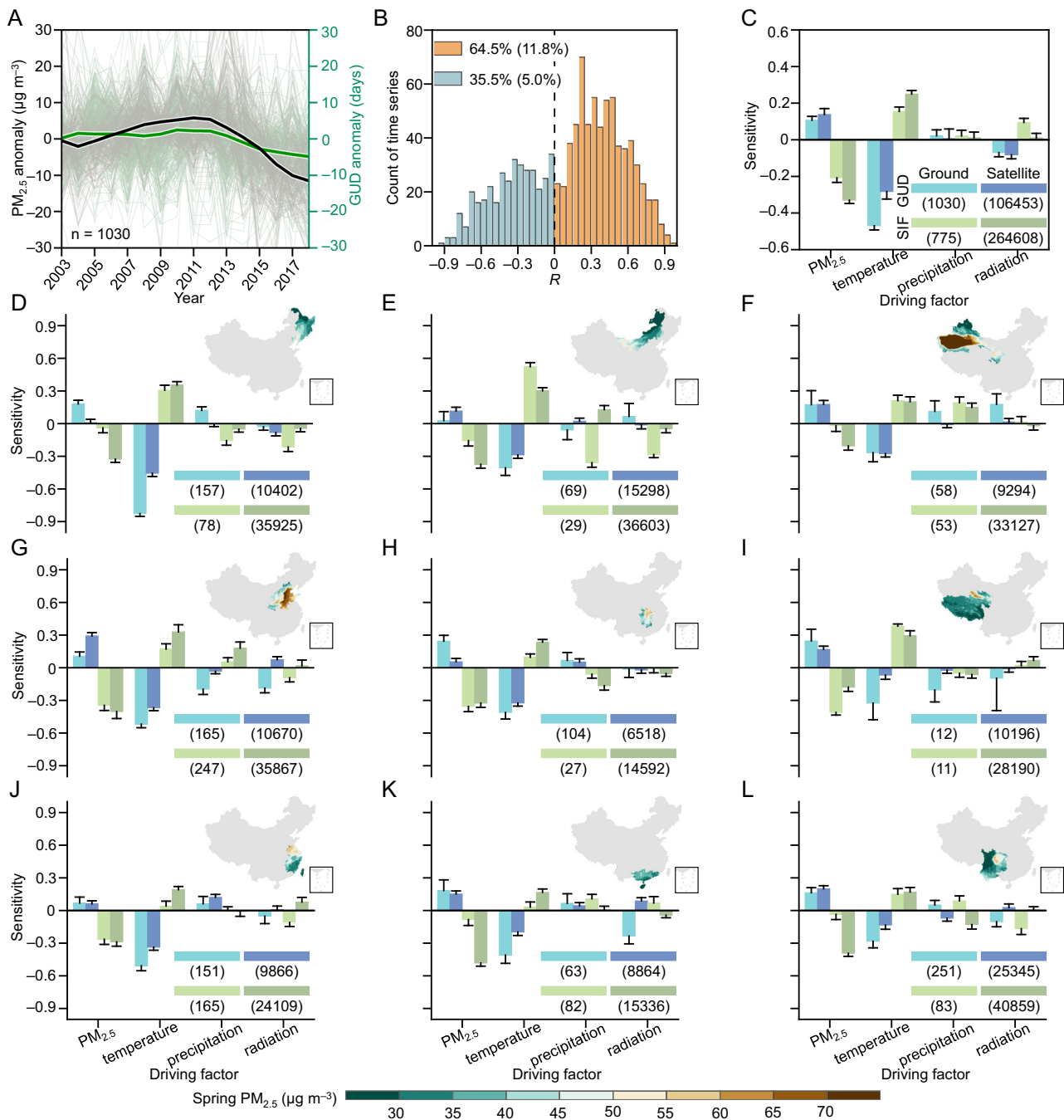


**Fig. 1 | The effects of PM<sub>2.5</sub> pollution on spring green-up date (GUD) and solar-induced fluorescence (SIF).** **A** Variations of the anomaly of spring PM<sub>2.5</sub> (March–May) and ground GUD from 2003 to 2018. The bold lines represent the trends of yearly mean values of the anomaly of spring PM<sub>2.5</sub> and GUD across all sites and species smoothed by an adjacent averaging method. **B** The distribution of partial correlation coefficient (*R*) between PM<sub>2.5</sub> and ground GUD. The effects of climatic factors (i.e., temperature, precipitation, and radiation) were removed for partial correlation analysis. The values in brackets represent frequencies of sites with significantly positive and negative partial correlations, respectively ( $p < 0.05$ ). **A**

two-sided *t*-test was used to assess the significance of the partial correlation analysis. **C** Sensitivities of GUD and SIF to PM<sub>2.5</sub> pollution and climatic factors for ground- and satellite-based analyses using ridge regression (unitless). **D–L** Regional results for northeastern China, Inner Mongolia, northwestern China, northern China, central China, the Tibetan Plateau, southeastern China, southern China, and southwestern China, respectively. Data are presented as mean values ± 95% CIs of sensitivities for C–L. The numbers in brackets represent the number of sites or pixels in the corresponding region. Source data are provided as a Source Data file.

development, influence regional ecosystem functioning and contribute to climate change. Given the strong association between high PM<sub>2.5</sub> pollution, industrialization, and urbanization<sup>13</sup>, these results hold key environmental implications for the disparities across population and income groups<sup>27</sup>. They also underscore the urgent need to reduce air pollution to mitigate the environmental consequences of human activity.

We identified specific mechanisms that explain how PM<sub>2.5</sub> contamination leads to a later spring GUD. High concentrations of PM<sub>2.5</sub> significantly increase chilling demands in winter and early spring, which may cause insufficient chilling for spring leaf unfolding<sup>28</sup>. Insufficient chilling causes a higher heat requirement for spring leaf unfolding, resulting in delayed GUD<sup>29</sup>. Such results were supported by the SEM analysis, which shows that the regulation of chilling

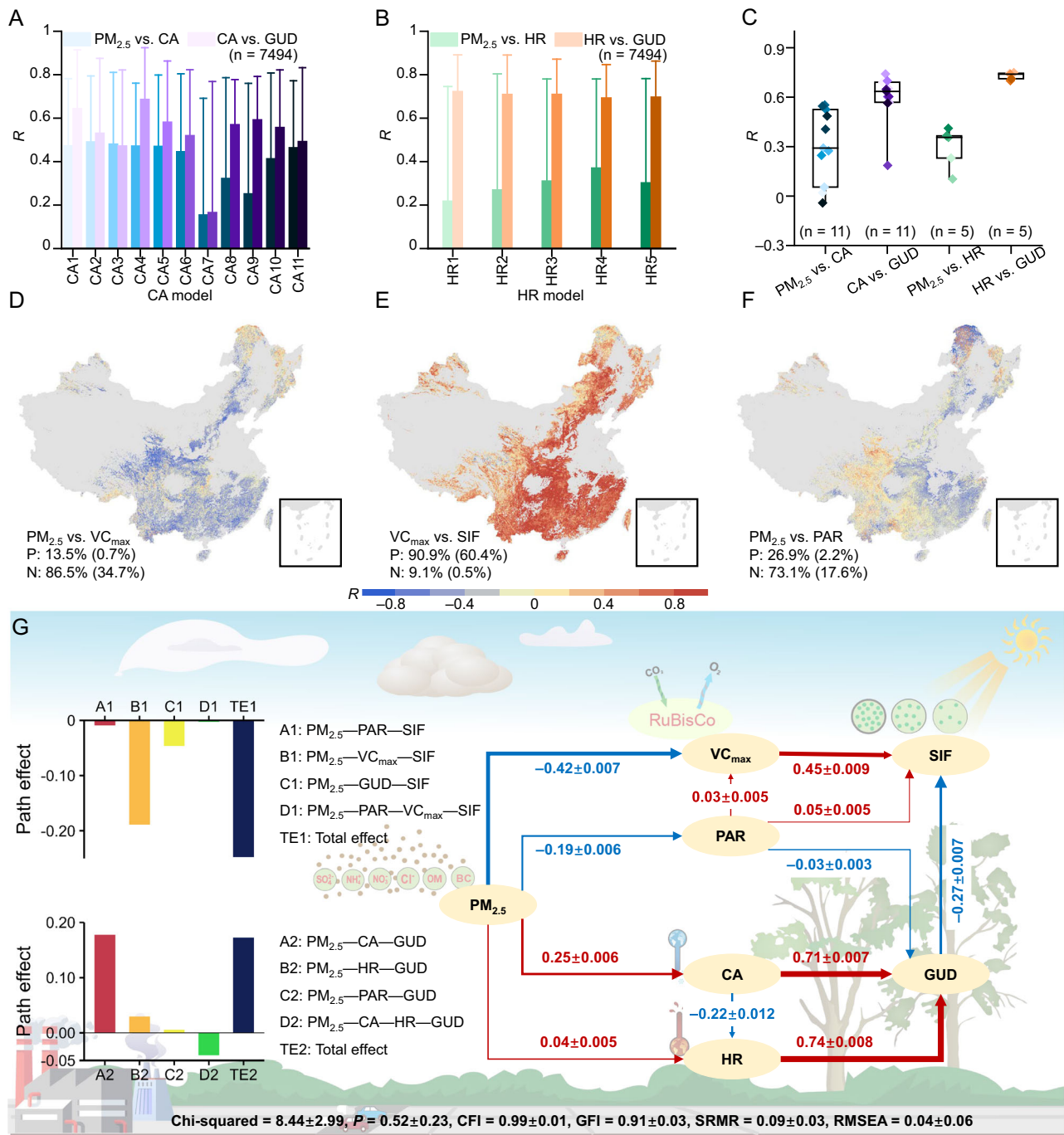


**Fig. 2 | Potential mechanisms underlying the correlation between spring greening and PM<sub>2.5</sub> pollution.** **A–C** The effects of PM<sub>2.5</sub> on chilling accumulation (CA), heat requirement (HR), and green-up date (GUD). The CA and HR were simulated by 11 CA models and five HR models (Methods). **A, B** represent PM<sub>2.5</sub>-CA-GUD and PM<sub>2.5</sub>-HR-GUD associations for satellite-based analyses. Data are presented as mean values + SDs of correlation coefficients (*R*). The numbers in brackets represent the number of pixels (*n*). **C** Represents associations for ground-based analyses. The correlations were determined by partial correlation analyses. Box plots display medians (horizontal lines), the 25th and 75th percentiles (box edges), and minimum and maximum values (whiskers). The numbers in brackets represent the number of models (*n*). The patterns of partial correlations: PM<sub>2.5</sub>

versus the maximum rate of carboxylation (VC<sub>max</sub>) (**D**), VC<sub>max</sub> versus solar-induced fluorescence (SIF) (**E**), and PM<sub>2.5</sub> versus photosynthetically active radiation (PAR) (**F**). *P* and *N* indicate positive and negative correlations, respectively. The values in the brackets represent the frequency of pixels with significant correlations (*p* < 0.05). **G** Structural equation model (SEM) describing the biogeophysical and biogeochemical relationships between PM<sub>2.5</sub> pollution and spring greening. Red and blue values indicate positive and negative correlations, respectively; numbers represent the means ± 95% CIs of standardized direct path coefficients under two-sided Wald test. The Chi-square test for model fit was one-sided. The arrow widths reflect the strength of the relationships. The criteria for evaluating SEM can be seen in “Methods”. Source data are provided as a Source Data file.

accumulation appears to have much larger path effects than other paths. Of comparable importance to CA, the adverse effects of PM<sub>2.5</sub> on VC<sub>max</sub>, which is one of the most important drivers of leaf photosynthetic capacity, explains the decline in spring SIF under high PM<sub>2.5</sub> pollution.

The Chinese government’s Air Pollution Prevention and Control Action Plan (APPCAP) from 2013-2017 represents the most significant effort to combat air pollution in China to date, as it covers more than 300 cities and involves multiple sectors, including energy, industry, transport, legal, and regulatory sectors<sup>30</sup>. Our study predicts that



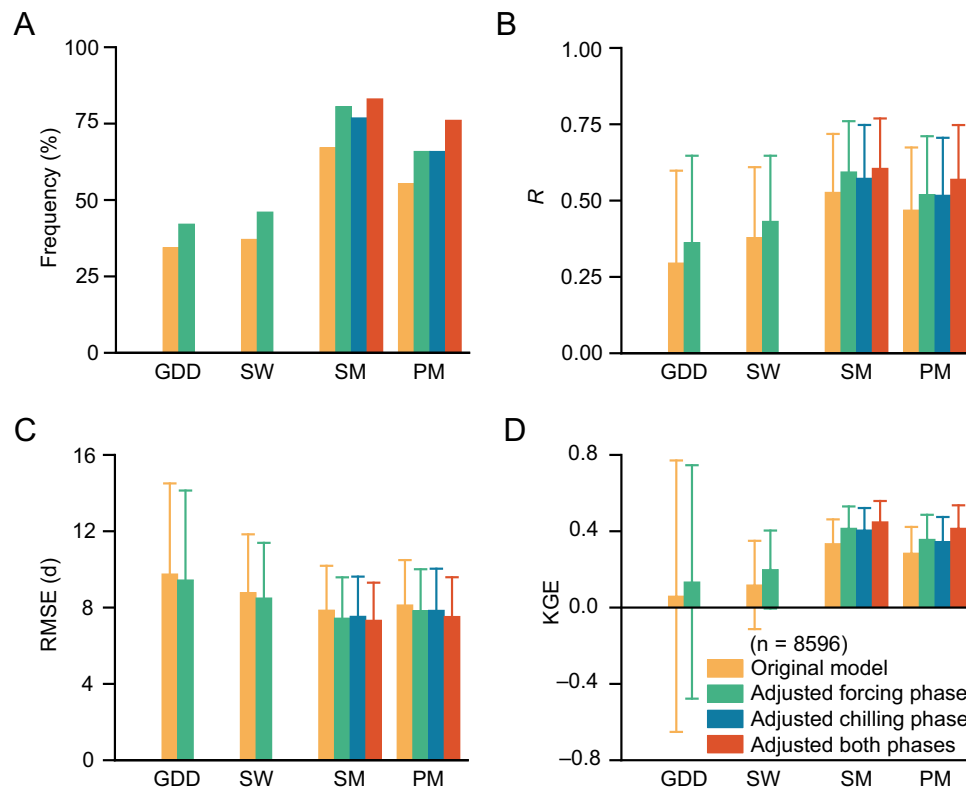


**Fig. 3 | Comparison of modeling of spring green-up date (GUD) before and after considering  $PM_{2.5}$  pollution effects.** A–D Results represent the percentages of pixels with significant correlations between model estimates and satellite observations of GUD (A), the average correlation coefficient ( $R$ ) (B), the average root mean square error (RMSE) (C), and the Kling-Gupta efficiency (KGE) (D), respectively, using the growing degree days (GDD), spring warming (SW), the sequential

model (SM) and the parallel model (PM) and corresponding revised model with  $PM_{2.5}$  effects in chilling, forcing, and both phases. Significance was set as  $p < 0.05$ . A two-sided  $t$ -test was used to assess the significance of the correlation analysis. Data are presented as mean values  $\pm$  SDs for (B–D). The legend in (D) applies to all panels. The number in bracket represents the number of pixels ( $n$ ). Source data are provided as a Source Data file.

earlier spring GUD will be hindered in the future if  $PM_{2.5}$  pollution is not properly addressed, resulting in a less green China than current expectations. This finding is particularly important as China, the largest emitter of  $CO_2$  in the world, has set ambitious goals to achieve peak  $CO_2$  emissions by 2030 and carbon neutrality by 2060<sup>31,32</sup>. The success of these goals will be supported by an alleviated offset in spring greening due to air pollution control, which is crucial for reducing  $CO_2$  emissions via photosynthesis processes. Our findings have far-reaching implications for policy design and implementation, emphasizing the synergies and trade-offs among multiple policies aimed at achieving sustainable development amid social and climate change. Beyond this, this study underscores the regulation of  $PM_{2.5}$  on C cycling, highlighting the potential uncertainties of future climate projections<sup>33,34</sup>. In conclusion, our findings are of significant value as they identify the crucial role of atmospheric pollution on spring GUD and productivity, providing essential insights for promoting comprehensive and sustainable development in China and the world.

## Methods

### In situ GUD records

We gathered and utilized all available in situ records for ground GUD (also known as leaf unfolding date) in China from the Chinese Phenological Observation Network (CPON)<sup>24</sup>, which has compiled phenological data since 1963 for 112 plant species across 145 sites nationwide. In CPON, spring GUD is defined as the date when leaves begin to unfold.

To detect and eliminate possible outliers of ground GUD, we applied the median absolute deviation (MAD) method, which is more resilient to outliers in a data set than the standard deviation. For each

site and species, MAD of GUD dataset ( $GUD_1, GUD_2, \dots, GUD_i$ ) can be expressed as:

$$MAD = \text{median}(|GUD_i - \text{median}(GUD)|) \quad (1)$$

For each site and species, any data record with more than 2.5 times MAD was removed as an outlier<sup>10</sup>. We also excluded all GUD records that were shorter than 15 years to make temporal analyses more reliable. In this way, we used a total of 1030 time series from 35 sites and 505 species for 2003–2018. The distribution and descriptions of the in situ data are detailed in Supplementary Fig. 1 and Table 2.

### Satellite-derived GUD observations

We applied satellite-derived spring GUD from 2001 to 2021, obtained from the Terra and Aqua combined Moderate Resolution Imaging Spectroradiometer (MODIS) Land Cover Dynamics (MCD12Q2) Version 6.1 data product<sup>25</sup> (Supplementary Table 1). This product uses the two-band Enhanced Vegetation Index (EVI2) to provide yearly metrics of global terrestrial surface phenology with an initial spatial resolution of  $500 \times 500$  m. For each pixel, satellite GUD was defined as the date when EVI2 first crossed 15% of the segment EVI2 amplitude. We implemented quality control measures to reduce uncertainties, and we removed GUD dates before 1 February or later than 30 June<sup>35</sup>. We downloaded, processed, and resampled the satellite GUD data into  $0.05 \times 0.05$  degree at the Google Earth Engine platform.

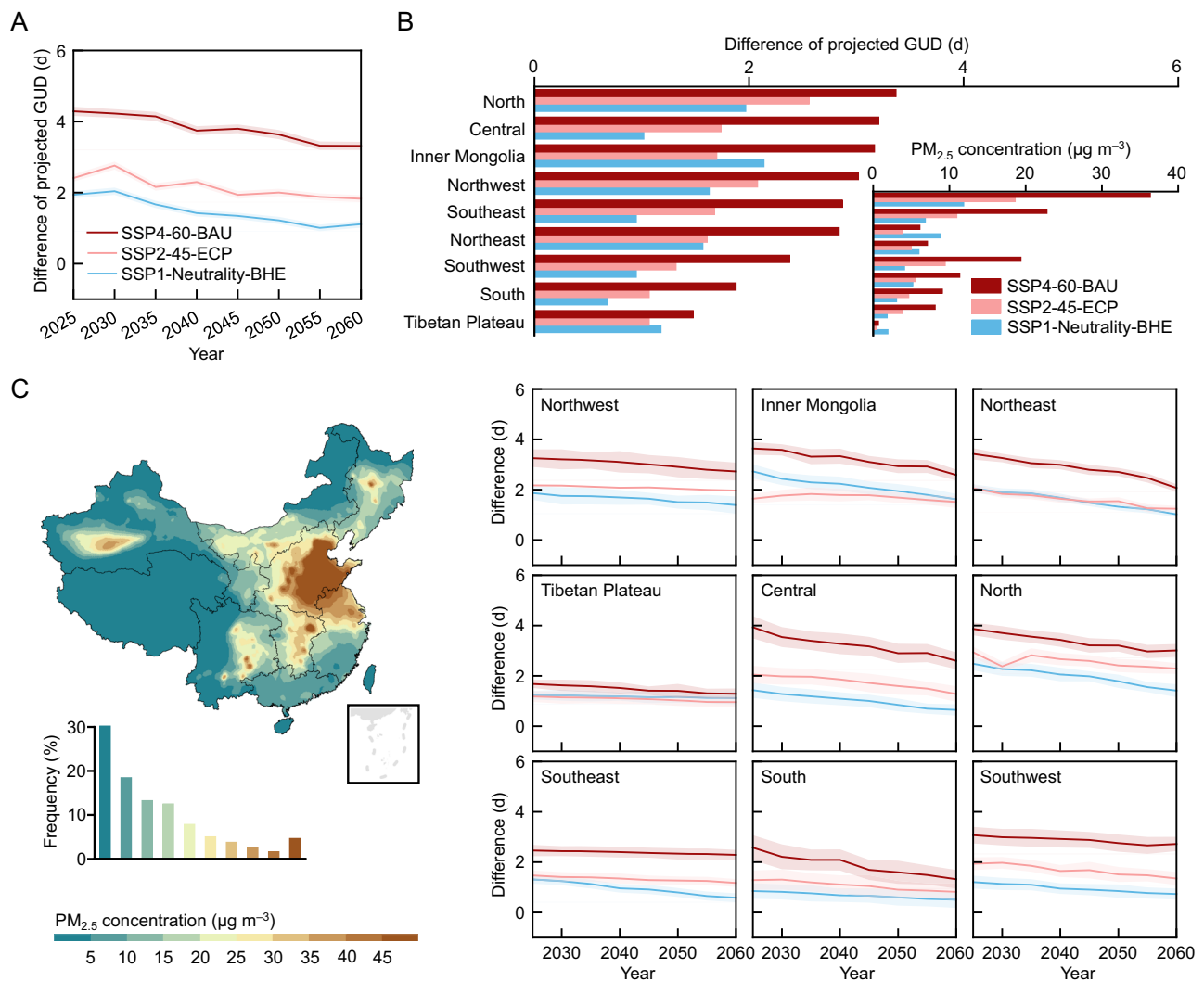


**Fig. 4 | Projections of spring green-up dates (GUD) under future emission and climate scenarios.** **A** Variations of the differences of the projected GUD using  $PM_{2.5}$ -weighted sequential model ( $SM_{PM}$ ) and original sequential model (SM) under different emission scenarios over 2025–2060. SSP1-Neutrality-BHE, SSP2-45-ECP, and SSP4-60-BAU represent scenarios of the neutral (the lowest), the current goal (middle), and a baseline goal (the highest) of  $PM_{2.5}$  pollution, respectively. **B** Multi-year mean differences of the projected GUD ( $SM_{PM}$  minus SM) and multi-year mean

spring  $PM_{2.5}$  under different scenarios for the nine main regions in China. **C** The left map shows the spatial pattern of multi-year averaged  $PM_{2.5}$  for winter and spring under the SSP4-60-BAU scenario. The right trends indicate the differences in projected GUD ( $SM_{PM}$  minus SM) across various emission scenarios from 2025 to 2060 for nine major regions in China. The legend in (A) applies to (C). Data are presented as mean values (bold lines)  $\pm$  95% CIs (error bands) for (A, C). Source data are provided as a Source Data file.

### Satellite-derived SIF observations

We used the long-term contiguous SIF (LCSIF) dataset (2001–2021)<sup>26</sup>. The dataset is accessible at a bi-monthly temporal resolution, accompanied by a spatial resolution of  $0.05 \times 0.05$  degree (Supplementary Table 1). The LCSIF showed strong correlations with satellite-based SIF observations from the Orbiting Carbon Observatory-2 (OCO-2) and ground-based estimates of gross primary productivity across different vegetation types, demonstrating its ability to accurately represent terrestrial photosynthesis. To examine  $PM_{2.5}$ -induced SIF signal attenuation, we calculated relative SIF, which refers to SIF normalized by the continuum-level NIR-reflected radiance, to check the response of SIF to  $PM_{2.5}$  pollution. We found overall consistent patterns of both  $PM_{2.5}$  and temperature sensitivities of SIF and relative SIF (Supplementary Fig. 9). These results indicated that the widespread decreases in spring SIF under  $PM_{2.5}$  pollution are primarily attributed to the biophysical effects of  $PM_{2.5}$  pollution rather than being influenced by signal attenuation<sup>22</sup>.

### Satellite-driven $PM_{2.5}$ data and evaluation

Daily and monthly satellite-driven  $PM_{2.5}$  data was obtained from the China High Air Pollutants (CHAP, version 4) dataset, covering the period 2001 to 2021, with a spatial resolution of  $1 \times 1$  km<sup>23</sup>. The CHAP data was derived by combining the MODIS Collection 6 MAIAC AOD product (MCD19A2) with information on meteorology, surface conditions, pollutant emission, and population distribution using the Space-Time Extra-Trees model. To evaluate the satellite-driven  $PM_{2.5}$  data, we used a ground monitoring network of  $PM_{2.5}$  observations with 1599 sites (at least 5-year records) in China from 2013 to 2021 (Supplementary Fig. 1). We evaluated the satellite-based spring and winter averaged  $PM_{2.5}$  concentrations using all collected site monitoring data, with  $R^2$  of 0.85 and 0.82 and RMSE of 6.89 and 11.74  $\mu g m^{-3}$  for spring and winter, respectively (Supplementary Fig. 10). The high accuracy of satellite-based  $PM_{2.5}$  data allows us to examine the response of spring vegetation activity to  $PM_{2.5}$  pollution. To match the spatial resolution of satellite GUD and SIF, we resampled satellite-driven  $PM_{2.5}$  data into  $0.05 \times 0.05$  degree.

**Future PM<sub>2.5</sub> simulations**

We simulated future PM<sub>2.5</sub> data from 2025 to 2060 at 5-year intervals under three emission scenarios: SSP1-Neutrality-BHE (best-health-effect scenario), SSP2-45-ECP (enhanced-control-policy scenario), and SSP4-60-BAU (business-as-usual scenario), using the Nested Air Quality Prediction Modeling System (NAQPMS)<sup>36</sup> (Supplementary Fig. 11). The PM<sub>2.5</sub> output has a horizontal resolution of 45 km and a temporal resolution of 6 h. Future emission inventories under the three scenarios were obtained from the Dynamic Projection Model for Emissions in China (DPEC v1.0, <http://meicmodel.org/>)<sup>37</sup>. Meteorological fields were provided by the Weather Research and Forecasting Model (WRF, version 3.6.1, available at <https://www.mmm.ucar.edu/weather-research-and-forecasting-model>). Initial and boundary conditions for four future climate scenarios (SSP1-19, SSP1-26, RCP4.5, and RCP6.0) were provided by Phases 5 and 6 of the Coupled Model Inter-comparison Project (CMIP5 and CMIP6). A summary of the future emissions and climate scenarios is provided in Supplementary Table 3.

**Climatic data and ancillary data**

Monthly meteorological data at a 1/24 degree resolution, including mean temperature and total precipitation, were obtained from TerraClimate<sup>38</sup> for 2001-2021. Since spring vegetation activity could be positively regulated by solar radiation and PM<sub>2.5</sub> could directly reduce the radiation, here we used cloudiness (0-100%) data derived from the Climate Research Unit (CRU TS v4.07) to represent the level of radiation (Supplementary Table 1)<sup>39</sup>. In our analyses, we negated the value of cloudiness sensitivity as radiation sensitivity (multiplied by -1) to make it more understandable. We obtained CN05.1 gridded daily mean temperature with a spatial resolution of 0.25°, derived from the National Meteorological Information Center of China, to calculate CA and HR, and to build and improve GUD models<sup>40</sup>. To exclude the impact of human activity on agricultural ecosystems, we removed all cropland areas using the MCD12Q1 MODIS land-cover product (collection 6) (Supplementary Fig. 1).

**Chilling models and forcing models**

We used 11 chilling models (C<sub>1</sub>-C<sub>11</sub>) and five forcing models (F<sub>1</sub>-F<sub>5</sub>) to quantify CA and HR, respectively<sup>26</sup>. Models C<sub>1</sub>-C<sub>6</sub> were developed based on various combinations of the upper and lower temperature limits. The equations for Models C<sub>1</sub>-C<sub>6</sub> are as follows:

$$CU_1 = \begin{cases} 1 & T \leq 5 \\ 0 & T > 5 \end{cases} \quad (2)$$

$$CU_2 = \begin{cases} 1 & -10 \leq T \leq 5 \\ 0 & T > 5 \text{ or } T < -10 \end{cases} \quad (3)$$

$$CU_3 = \begin{cases} 1 & 0 \leq T \leq 5 \\ 0 & T > 5 \text{ or } T < 0 \end{cases} \quad (4)$$

$$CU_4 = \begin{cases} 1 & T \leq 7 \\ 0 & T > 7 \end{cases} \quad (5)$$

$$CU_5 = \begin{cases} 1 & -10 \leq T \leq 7 \\ 0 & T > 7 \text{ or } T < -10 \end{cases} \quad (6)$$

$$CU_6 = \begin{cases} 1 & 0 \leq T \leq 7 \\ 0 & T > 7 \text{ or } T < 0 \end{cases} \quad (7)$$

where CU<sub>*i*</sub> is the rate of chilling for Model C<sub>*i*</sub>, and *T* is the daily mean temperature (°C).

Models C<sub>7</sub> and C<sub>8</sub> were designed by assigning different weights to different ranges of temperatures<sup>41</sup>. Models C<sub>9</sub>-C<sub>11</sub> have triangular forms designed for multiple plant species<sup>42</sup>. The equations for Models C<sub>7</sub>-C<sub>11</sub> are as follows:

$$CU_7 = \begin{cases} 0 & T \leq 1.4 \\ 0.5 & 1.4 < T \leq 2.4 \\ 1 & 2.4 < T \leq 9.1 \\ 0.5 & 9.1 < T \leq 12.4 \\ 0 & 12.4 < T \leq 15.9 \\ -0.5 & 15.9 < T \leq 18 \\ -1 & T > 18 \end{cases} \quad (8)$$

$$CU_8 = \begin{cases} 0 & T \leq 1.4 \\ 0.5 & 1.4 < T \leq 2.4 \\ 1 & 2.4 < T \leq 9.1 \\ 0.5 & 9.1 < T \leq 12.4 \\ 0 & T > 12.4 \end{cases} \quad (9)$$

$$CU_9 = \begin{cases} 1 & 2.5 < T < 7.4 \\ 0 & T < -4.7 \text{ or } T > 16 \\ 3.13 \times \left(\frac{T+4.66}{10.93}\right)^{2.10} \times e^{-\left(\frac{T+4.66}{10.93}\right)^{3.10}} & \text{else} \end{cases} \quad (10)$$

$$CU_{10} = \begin{cases} 0 & T \leq -3.4 \text{ or } T \geq 10.4 \\ \frac{T+3.4}{5+3.4} & -3.4 < T < 5 \\ \frac{T-10.4}{5-10.4} & 5 < T < 10.4 \end{cases} \quad (11)$$

$$CU_{11} = \begin{cases} 0 & T \leq -6.5 \text{ or } T \geq 6.9 \\ \frac{T+6.5}{6.9-0.2} & -6.5 < T \leq 0.2 \\ \frac{6.9-T}{6.9-0.2} & 0.2 < T < 6.9 \end{cases} \quad (12)$$

where CU<sub>*i*</sub> is the rate of chilling for Model C<sub>*i*</sub>, and *T* is the daily mean temperature (°C).

We used five widely used forcing models to measure the HR of GUD<sup>29,42</sup>. The growing degree days (GDD) model is the most commonly used forcing model, which assumes that the rate of forcing is linearly correlated with temperature if the temperature is above a particular threshold. The equations for models F<sub>1</sub>-F<sub>5</sub> are as follows:

$$FU_1 = \max(T, 0) \quad (13)$$

$$FU_2 = \max(T - 5, 0) \quad (14)$$

$$FU_3 = \begin{cases} \frac{28.4}{1 + e^{-0.185 \times (T - 18.5)}} & T > 0 \\ 0 & \text{else} \end{cases} \quad (15)$$

$$FU_4 = \frac{1}{1 + e^{-0.47 \times T + 6.49}} \quad (16)$$

$$FU_5 = \begin{cases} 0 & T < T_L \text{ or } T > T_c \\ \frac{T_u - T_L}{2} \times \left(1 + \cos\left(\pi + \pi \times \frac{T - T_L}{T_u - T_L}\right)\right) & T_L \geq T \geq T_u \\ (T_u - T_L) \times \left(1 + \cos\left(\frac{\pi}{2} + \frac{\pi}{2} \times \frac{T - T_u}{T_c - T_u}\right)\right) & T_u < T \leq T_c \end{cases} \quad (17)$$

where FU<sub>*i*</sub> is the rate of forcing for Model F<sub>*i*</sub>, and *T* is the daily mean temperature (°C). *T<sub>L</sub>* = 4, *T<sub>u</sub>* = 25, and *T<sub>c</sub>* = 36.

### Spring phenological models

In this study, we used four spring phenological models: the GDD and spring warming (SW) models (one-phase models), and the sequential model (SM) and parallel model (PM) (two-phase models)<sup>43</sup>. In all models, GUD was simulated as the date when the state of forcing ( $S_f$ ) reached its critical value ( $F_{crit}$ ). The primary differences among the models lay in the calculation of the daily rate of forcing ( $R_f$ ) and the conditions required for the accumulation to start.

$$S_f = \sum_{t_0}^t R_f \tag{18}$$

$$\text{GUD} = t, \text{ if } S_f \geq F_{crit} \tag{19}$$

The one-phase models solely accounted for the influence of forcing and calculated  $R_f$  starting from 1 January of the current year ( $t_0$ ) (Eq. 18). The date when  $S_f$  exceeds  $F_{crit}$  is regarded as the GUD.

The GDD model begins to accumulate  $R_f$  when the temperature reaches a baseline threshold ( $T_{baseline}$ ):

$$R_f = \begin{cases} 0 & T \leq T_{baseline} \\ T & T > T_{baseline} \end{cases} \tag{20}$$

The SW model calculates the  $R_f$  based on a logistic function:

$$R_f = \frac{A_f}{1 + e^{\alpha(T - \beta)}} \tag{21}$$

where  $A_f$ ,  $\alpha$  and  $\beta$  are process-specific parameters to be determined.

The two-phase SM and PM, in contrast to the one-phase models, assume that the accumulation of forcing cannot begin until a critical threshold ( $C_{crit}$ ) of the chilling state ( $S_c$ , a daily sum of chilling rates) is reached. A triangle function (Eq. 22) was used to describe the daily rate of chilling ( $R_c$ ), and  $S_c$  began to accumulate after 1 September of the preceding year ( $t_c$ ) (Eq. 23):

$$R_c = \begin{cases} 0, & T \leq T_a \\ \frac{T - T_a}{T_b - T_a}, & T_a < T \leq T_b \\ \frac{T - T_c}{T_b - T_c}, & T_b < T < T_c \\ 0, & T \geq T_c \end{cases} \tag{22}$$

$$S_c = \sum_{t_c}^t R_c \tag{23}$$

where  $T_a$ ,  $T_b$  and  $T_c$  are the threshold temperatures at which the state of  $R_c$  changes during the chilling accumulation process.

The forcing phase of the SM was similar to that of the SW model using  $R_f$ , but with an adjustment factor,  $K$ , to ensure that the accumulation of forcing occurs after the chilling state ( $C_{crit}$ ) is fulfilled (Eq. 24). Like the GDD model, the SM also uses a temperature threshold ( $T_d$ ) to establish the requirement for beginning the accumulation of forcing (Eq. 8) and meeting  $C_{crit}$ .

$$K = \begin{cases} 0 & S_c < C_{crit} \\ 1 & S_c \geq C_{crit} \end{cases} \tag{24}$$

$$R_f = \begin{cases} 0 & T \leq T_d \\ K \times \frac{A_f}{1 + e^{\alpha(T - \beta)}} & T > T_d \end{cases} \tag{25}$$

The PM is a modified version of the SM that assumes that the accumulation of forcing is not strictly zero before  $C_{crit}$  is achieved. The only difference between the parameters of the SM and the PM is how  $K$  is calculated (Eq. 26). The PM adds a new parameter ( $K_{min}$ ), which calculates the minimal potential of a bud that has not been chilled to react to the forcing temperature<sup>39,40</sup>.

$$K = \begin{cases} K_{min} + \frac{1 - K_{min}}{C_{crit}} \times S_c & S_c < C_{crit} \\ 1 & S_c \geq C_{crit} \end{cases} \tag{26}$$

The improved models were developed by incorporating the daily  $PM_{2.5}$  data into the above models, i.e., GDD, SW, SM, and PM. We added two new parameters ( $K_{chilling}$ ,  $K_{forcing}$ ), together with the normalized difference of daily  $PM_{2.5}$  concentration (NDPM, Eq. 27), to these new models to modify the  $R_c$  and  $R_f$  using an exponential function (Eqs. 28, 29), accounting for how  $PM_{2.5}$  regulates CA and HR before the leaf green-up. For one-phase models (i.e., GDD and SW), we modified the daily rate of forcing. For two-phase models (i.e., SM and PM), we modified rates of chilling and forcing.

$$\text{NDPM}_{t_i} = \frac{PM_{2.5}_{t_i} - \min(PM_{2.5})}{\max(PM_{2.5}) - \min(PM_{2.5})} \tag{27}$$

$$S_{PM_{2.5-c}} = \sum_{t_0}^t R_{PM_{2.5-c}} = \sum_{t_0}^t R_c \times F_{PM_{2.5-c}} = \sum_{t_0}^t R_c \times e^{K_{chilling} \times \text{NDPM}_{t_i}} \tag{28}$$

$$S_{PM_{2.5-f}} = \sum_{t_0}^t R_{PM_{2.5-f}} = \sum_{t_0}^t R_f \times F_{PM_{2.5-f}} = \sum_{t_0}^t R_f \times e^{K_{forcing} \times \text{NDPM}_{t_i}} \tag{29}$$

where  $PM_{2.5}$  represents daily  $PM_{2.5}$  concentration,  $\text{NDPM}_{t_i}$  represents the normalized difference of daily  $PM_{2.5}$  concentration of  $t_i$ .  $S_{PM-c}$  and  $S_{PM-f}$  represent the  $PM_{2.5}$ -adjusted  $S_c$  and  $S_f$ , respectively.  $t_0$  and  $t$  represent the start and end days of chilling (Eq. 28) and forcing (Eq. 29), respectively.

We implemented the Particle Swarm Optimization (PSO) algorithm at each pixel or site to iteratively calculate a set of optimal model parameters for each spring phenology model, using satellite and ground GUD data and daily air temperature. The nature-based PSO algorithm is one of the most widely used swarm intelligence algorithms, in which individuals are referred to as particles and seek the search space for the global optimal position that minimizes (or maximizes) a given problem<sup>44,45</sup>. The set of optimal parameters was selected when RMSE between the modeled and observed GUD was lowest<sup>43</sup>. We further checked the patterns of  $PM_{2.5}$ -weighted parameters ( $K_{chilling}$  and  $K_{forcing}$ ). We found that  $K_{chilling}$  was positive at 54.6% of the area, nearly five times the negative value (Supplementary Fig. 12), confirming that  $PM_{2.5}$  pollution reduced the efficiency of CA.

To evaluate the GUD models, we calculated the frequency of pixels with significant correlations between model estimates and observations, the correlation coefficient ( $R$ ), the root mean square error (RMSE), and the Kling-Gupta efficiency (KGE) using both ground and satellite GUD.

### Analyses

**Response of spring GUD and SIF to  $PM_{2.5}$  pollution.** We conducted site-level and grid-level analyses for ground and satellite observations. For site-level analyses, we used ground GUD derived from the CPON and  $PM_{2.5}$  and climatic data for the same location extracted from gridded products. We also extracted satellite SIF for all GUD sites to determine site-level climatic and  $PM_{2.5}$  sensitivities. For grid-level analyses, we used satellite GUD, SIF, and gridded climatic and  $PM_{2.5}$  data with a consistent spatial resolution ( $0.05 \times 0.05$  degree) resampled by the bilinear interpolation method. We applied the Theil-Sen



slope estimator to analyze the temporal patterns of spring GUD, SIF, and  $PM_{2.5}$ , evaluated by the Mann–Kendall trend test at a significance level of 0.05. We found overall advancing trends of GUD, increasing trends of SIF, and decreasing trends of  $PM_{2.5}$  concentration (Supplementary Fig. 13) for 2001–2021, indicating the synergistic changes in  $PM_{2.5}$  pollution and spring vegetation activities and their potential interplays.

To avoid potential multicollinearity between climatic factors and  $PM_{2.5}$  concentration, we applied ridge regression, which incorporates a penalty parameter to reduce the variance of regression coefficients. This approach was used to determine the sensitivities of GUD and SIF to  $PM_{2.5}$  pollution and climatic factors (i.e., temperature, precipitation, and radiation). To isolate the effects of  $PM_{2.5}$  and climatic factors on GUD, we first conducted partial correlation analyses to calculate the optimal length of pre-season of each factor for each site or pixel. For each factor, the optimal pre-season was defined as the period before the GUD with the highest absolute partial correlation coefficient between GUD and corresponding factors. We then calculated the  $PM_{2.5}$  and climatic sensitivities as the coefficients of the ridge regression between the GUD and the averaged  $PM_{2.5}$ , temperature, radiation, and accumulated precipitation during the pre-season periods for corresponding driving factors<sup>10</sup>. It should be noted that ridge-regression-based sensitivities are unitless since we used normalized anomalies of all variables mentioned above. Positive sensitivities indicate delayed GUD, while negative sensitivities suggest advanced GUD.

To determine the environmental responses of spring SIF, we applied the ridge regression method, with spring mean SIF as the response variable and spring averaged  $PM_{2.5}$ , temperature, radiation, and accumulated precipitation as predictors. It should be noted that cloudiness (the proxy of radiation) could be potentially impacted by heavy  $PM_{2.5}$  pollution due to aerosol–cloud interactions<sup>46</sup>, further influencing precipitation and even temperature. We used partial correlation analyses and ridge regression methods to minimize the potential multicollinearity between climatic factors and  $PM_{2.5}$  concentration and to focus on the  $PM_{2.5}$  effects on spring vegetation activity. Future investigations on the interactive effects of climate change and  $PM_{2.5}$  pollution are potentially needed. Here, we also examined the impact of  $PM_{2.5}$  on near-surface temperature using weather station records from 633 sites (Supplementary Table 1). We found that  $PM_{2.5}$  had varying impacts on daily mean, maximum, and minimum temperatures in spring: while it slightly increased daily mean and maximum temperatures, it did not affect daily minimum temperature (Supplementary Fig. 14). These results indicate a limited regulatory role of  $PM_{2.5}$  on temperature.

**Potential mechanisms under  $PM_{2.5}$  effects.** We investigated the biogeochemical and biogeophysical mechanisms underlying the effects of  $PM_{2.5}$ . We first checked the impacts of  $PM_{2.5}$  on the CA derived from 11 models and HR derived from five models. Given that CA may be influenced by temperature variations, we conducted partial correlation analyses to examine the relationship between  $PM_{2.5}$  and CA while controlling for temperature effects during CA periods. Previous studies have shown a negative correlation between CA and HR<sup>28,47</sup>, which aligns with our SEM analysis results (Fig. 2G). To assess the impact of  $PM_{2.5}$  on HR, we also performed partial correlation analyses, controlling for temperature effects during HR periods and preceding CA. Since CA and HR jointly and interactively influence GUD, we used partial correlation analyses to explore the CA–GUD and HR–GUD relationships, excluding the effects of HR and CA, respectively.

We introduced PAR<sup>48</sup> and  $VC_{max}$ <sup>49</sup>, together with GUD, to explain  $PM_{2.5}$ 's effects on SIF. We used partial correlation analyses to examine associations between  $PM_{2.5}$  and PAR and  $VC_{max}$ , as well as between  $VC_{max}$  and SIF (Fig. 2D–F). The data description of PAR and  $VC_{max}$  can be seen in Supplementary Table 1. We also considered  $PM_{2.5}$  effects on

diffuse PAR<sup>48</sup>, and its association with SIF (Supplementary Fig. 6). It should be noted that the modeled  $VC_{max}$  we used has been evaluated using measurements of leaf chlorophyll and  $VC_{max}$  across different species and vegetation types<sup>50,51</sup>. In the last step, we applied Structural Equation Models (SEM) to investigate the biogeophysical (through CA and HR) and biogeochemical (through  $VC_{max}$  and PAR) effects of  $PM_{2.5}$  pollution on spring GUD and SIF (Fig. 3C–H). The SEM allows us to quantify both direct and indirect causal relationships among multiple driving factors. Utilizing multiple gridded variables, our SEM elucidated the mechanisms of distinct negative influences of  $PM_{2.5}$  pollution on spring greening. All variables were standardized before analyses, and maximum-likelihood estimation was used to calculate the path coefficients. We used the standard criteria to assess the validity of our SEM, including the  $\chi^2$  test ( $p > 0.05$ ), the comparative fit index (CFI  $> 0.9$ ), the Standardized Root Mean Square Residual (SRMR  $< 0.08$ ), the goodness of fit index (GFI  $> 0.95$ ), and the Root Mean Square Error of Approximation (RMSEA  $< 0.08$ ). We conducted SEM for each pixel, and the SEM was considered valid if at least three out of five criteria were met<sup>52</sup>. SEMs were constructed using the “lavaan” package in R<sup>53</sup>. To better disentangle the effects of  $PM_{2.5}$  and understand the underlying mechanisms, future investigations, especially simulation experiments that measure plant physiology and hormones under different levels of  $PM_{2.5}$  pollution, are essential.

### Reporting summary

Further information on research design is available in the Nature Portfolio Reporting Summary linked to this article.

### Data availability

All data used in this study are freely available from the following sources: Ground-based  $PM_{2.5}$  data are available from CNEMC, while satellite-derived  $PM_{2.5}$  data can be accessed from CHAP v4 (<https://zenodo.org/record/6398971>). Future  $PM_{2.5}$  input data were generated based on the climate projections from CMIP5 and CMIP6 future scenarios (<https://esgf-node.lnl.gov/projects/esgf-lnl/>). Ground-based GUD data are provided by the China Phenological Observation Network (CPON, <http://www.cpon.ac.cn/>), and satellite-based GUD data can be obtained from MCD12Q2 v6.1 (<https://lpdaac.usgs.gov/products/mcd12q2v061/>). SIF data are available from <https://zenodo.org/records/14568491>. Ground temperature data and CN05.1 data are accessible from <http://data.cma.cn/en>. The TerraClimate data can be accessed from [https://climate.northwestknowledge.net/TERRACLIMATE/index\\_animations.php/](https://climate.northwestknowledge.net/TERRACLIMATE/index_animations.php/). The CRU data can be accessed from <https://crudata.uea.ac.uk/cru/data/hrg/>.  $VC_{max}$  data are accessible from <https://www.nesdc.org.cn/sdo/detail?id=612f42ee7e28172cbcd3d80f>. PAR and PAR<sub>diff</sub> data can be obtained from <https://www.environment.snu.ac.kr/bess-rad>. Source data are provided with this paper.

### Code availability

All data analyses and modeling were performed using R 4.3.1. The code is stored in a publicly available Zenodo repository <https://zenodo.org/records/14826584>.

### References

1. IPCC. Summary for Policymakers. In: Climate Change 2023: Synthesis Report. Contribution of Working Groups I, II and III to the Sixth Assessment Report of the Intergovernmental Panel on Climate Change (eds Core Writing Team, Lee, H. & Romero, J.) 1–34 (IPCC, 2023). <https://doi.org/10.59327/IPCC/AR6-9789291691647.001>
2. Piao, S. et al. Characteristics, drivers and feedbacks of global greening. *Nat. Rev. Earth. Environ.* **1**, 14–27 (2020).
3. Zhu, Z. et al. Greening of the Earth and its drivers. *Nat. Clim. Chang.* **6**, 791–795 (2016).

4. Walther, G. R. et al. Ecological responses to recent climate change. *Nature* **416**, 389–395 (2002).
5. Chen, C. et al. China and India lead in greening of the world through land-use management. *Nat. Sustain.* **2**, 122–129 (2019).
6. Song, X. P. et al. Global land change from 1982 to 2016. *Nature* **560**, 639–643 (2018).
7. Peñuelas, J., Rutishauser, T. & Filella, I. Phenology feedbacks on climate change. *Science* **324**, 887–888 (2009).
8. Keenan, T. F. et al. Net carbon uptake has increased through warming-induced changes in temperate forest phenology. *Nat. Clim. Chang.* **4**, 598–604 (2014).
9. Fu, Y. H. et al. Declining global warming effects on the phenology of spring leaf unfolding. *Nature* **526**, 104–107 (2015).
10. Wang, J., Liu, D., Ciais, P. & Peñuelas, J. Decreasing rainfall frequency contributes to earlier leaf onset in northern ecosystems. *Nat. Clim. Chang.* **12**, 386–392 (2022).
11. Myneni, R. B., Keeling, C. D., Tucker, C. J., Asrar, G. & Nemani, R. R. Increased plant growth in the northern high latitudes from 1981 to 1991. *Nature* **386**, 698–702 (1997).
12. Yue, H., He, C., Huang, Q., Yin, D. & Bryan, B. A. Stronger policy required to substantially reduce deaths from PM<sub>2.5</sub> pollution in China. *Nat. Commun.* **11**, 1462 (2020).
13. McDuffie, E. E. et al. Source sector and fuel contributions to ambient PM<sub>2.5</sub> and attributable mortality across multiple spatial scales. *Nat. Commun.* **12**, 3594 (2021).
14. Xu, F. et al. The challenge of population aging for mitigating deaths from PM<sub>2.5</sub> air pollution in China. *Nat. Commun.* **14**, 5222 (2023).
15. Geng, G. et al. Drivers of PM<sub>2.5</sub> air pollution deaths in China 2002–2017. *Nat. Geosci.* **14**, 645–650 (2021).
16. Moreno-Mateos, D. et al. Anthropogenic ecosystem disturbance and the recovery debt. *Nat. Commun.* **8**, 14163 (2017).
17. Lin, Y., Zou, J., Yang, W. & Li, C. Q. A review of recent advances in research on PM<sub>2.5</sub> in China. *Int. J. Environ. Res. Public Health* **15**, 438 (2018).
18. Kok, J. F. et al. Smaller desert dust cooling effect estimated from analysis of dust size and abundance. *Nat. Geosci.* **10**, 274–278 (2017).
19. Kim, K. et al. PM<sub>2.5</sub> reduction capacities and their relation to morphological and physiological traits in 13 landscaping tree species. *Urban For. Urban Green.* **70**, 127526 (2022).
20. Holmes, C. Air pollution and forest water use. *Nature* **507**, E1–E2 (2014).
21. Li, Y., Wang, Y., Wang, B., Wang, Y. & Yu, W. The response of plant photosynthesis and stomatal conductance to fine particulate Matter (PM<sub>2.5</sub>) based on leaf factors analyzing. *J. Plant Biol.* **62**, 120–128 (2019).
22. He, L. et al. The weekly cycle of photosynthesis in Europe reveals the negative impact of particulate pollution on ecosystem productivity. *Proc. Natl Acad. Sci. USA* **120**, e2306507120 (2023).
23. Wei, J. et al. Reconstructing 1-km-resolution high-quality PM<sub>2.5</sub> data records from 2000 to 2018 in China: spatiotemporal variations and policy implications. *Remote Sens. Environ.* **252**, 112136 (2021).
24. Ge, Q., Wang, H., Rutishauser, T. & Dai, J. Phenological response to climate change in China: a meta-analysis. *Glob. Chang. Biol.* **21**, 265–274 (2015).
25. Friedl, M., Sulla-Menashe, D. Boston University and MODAPS SIPS—NASA. MCD12Q2 MODIS/Terra+Aqua Land Cover Dynamics Yearly L3 Global 500m SIN Grid. NASA LP DAAC. <https://doi.org/10.5067/MODIS/MCD12Q2.006> (2015).
26. Lian, X. et al. Diminishing carryover benefits of earlier spring vegetation growth. *Nat. Ecol. Evol.* **8**, 218–228 (2024).
27. Jbaily, A. et al. Air pollution exposure disparities across US population and income groups. *Nature* **601**, 228–233 (2022).
28. Wang, H. et al. Overestimation of the effect of climatic warming on spring phenology due to misrepresentation of chilling. *Nat. Commun.* **11**, 4945 (2020).
29. Fu, Y. H. et al. Increased heat requirement for leaf flushing in temperate woody species over 1980–2012: effects of chilling, precipitation and insolation. *Glob. Chang. Biol.* **21**, 2687–2697 (2015).
30. The State Council of China. Air Pollution Prevention and Control Action Plan. <http://www.gov.cn/jrzq/2013-09/12/> (2013).
31. Friedlingstein, P. et al. Global carbon budget 2020. *Earth Syst. Sci. Data.* **12**, 3269–3340 (2020).
32. Liu, Z. et al. Challenges and opportunities for carbon neutrality in China. *Nat. Rev. Earth. Environ.* **3**, 141–155 (2021).
33. Persad, G. G. & Caldeira, K. Divergent global-scale temperature effects from identical aerosols emitted in different regions. *Nat. Commun.* **9**, 3289 (2018).
34. Watson-Parris, D. & Smith, C. J. Large uncertainty in future warming due to aerosol forcing. *Nat. Clim. Chang.* **12**, 1111–1113 (2022).
35. Meng, L. et al. Urban warming advances spring phenology but reduces the response of phenology to temperature in the conterminous United States. *Proc. Natl Acad. Sci. USA* **117**, 4228–4233 (2020).
36. Wang, Z. et al. Modeling study of regional severe hazes over mid-eastern China in January 2013 and its implications on pollution prevention and control. *Sci. China Earth Sci.* **57**, 3–13 (2014).
37. Cheng, J. et al. Pathways of China’s PM<sub>2.5</sub> air quality 2015–2060 in the context of carbon neutrality. *Natl. Sci. Rev.* **8**, nwab078 (2021).
38. Abatzoglou, J. T., Dobrowski, S. Z., Parks, S. A. & Hegewisch, K. C. TerraClimate, a high-resolution global dataset of monthly climate and climatic water balance from 1958–2015. *Sci. Data.* **5**, 170191 (2018).
39. Harris, I., Jones, P. D., Osborn, T. J. & Lister, D. H. Updated high-resolution grids of monthly climatic observations—the CRU TS3.10 Dataset. *Int. J. Climatol.* **34**, 623–642 (2014).
40. Wu, J. & Gao, X. J. A gridded daily observation dataset over China region and comparison with the other datasets. *Chin. J. Geophys.* **56**, 1102–1111 (2013).
41. Luedeling, E., Zhang, M., Luedeling, V. & Girvetz, E. H. Sensitivity of winter chill models for fruit and nut trees to climatic changes expected in California’s Central Valley. *Agr. Ecosyst. Environ.* **133**, 23–31 (2009).
42. Hänninen, H. Modelling bud dormancy release in trees from cool and temperate regions. *Acta. For. Fenn.* **213**, 1–47 (1990).
43. Liu, Q., Fu, Y. H., Liu, Y., Janssens, I. A. & Piao, S. Simulating the onset of spring vegetation growth across the Northern Hemisphere. *Glob. Chang. Biol.* **24**, 1342–1356 (2018).
44. Poli, R., Kennedy, J. & Blackwell, T. Particle swarm optimization: an overview. *Swarm. Intell.* **1**, 33–57 (2007).
45. Zambrano-Bigiarini, M. & Rojas, R. A model-independent Particle Swarm Optimisation software for model calibration. *Environ. Model. Softw.* **43**, 5–25 (2013).
46. Zhao, B. et al. Enhanced PM<sub>2.5</sub> pollution in China due to aerosol-cloud interactions. *Sci. Rep.* **7**, 4453 (2017).
47. He, L. et al. Non-symmetric responses of leaf onset date to natural warming and cooling in northern ecosystems. *PNAS nexus* **2**, pgad308 (2023).
48. Ryu, Y., Jiang, C., Kobayashi, H. & Detto, M. MODIS-derived global land products of shortwave radiation and diffuse and total photosynthetically active radiation at 5 km resolution from 2000. *Remote Sens. Environ.* **204**, 812–825 (2018).
49. Lu, X. et al. Maximum carboxylation rate estimation with Chlorophyll content as a proxy of Rubisco content. *J. Geophys. Res. Biogeosci.* **125**, e2020JG005748 (2020).
50. Lu, X. et al. Estimating photosynthetic capacity from optimized Rubisco–chlorophyll relationships among vegetation types and under global change. *Environ. Res. Lett.* **17**, 014028 (2022).
51. Qian, X. et al. Relationship between leaf maximum carboxylation rate and chlorophyll content preserved across 13 species. *J. Geophys. Res.: Biogeosci.* **126**, e2020JG006076 (2021).

52. Bagozzi, R. P. & Yi, Y. Specification, evaluation, and interpretation of structural equation models. *J. Acad. Mark. Sci.* **40**, 8–34 (2012).
53. Rosseel, Y. lavaan: an R package for structural equation modeling. *J. Stat. Soft.* **48**, 1–36 (2012).

## Acknowledgements

This work was funded by the Third Xinjiang Scientific Expedition of the Ministry of Science and Technology of the PRC (2022xjkk0904) and the National Natural Science Foundation of China (42125101, 42401029). W.Q. was funded by China Postdoctoral Science Foundation (O7Z76126Z1). C.M.Z. was funded by SNF Ambizione grant PZ00P3\_193646. J.P. was funded by the TED2021-132627B-I00 grant funded by the Spanish MCIN, AEI/ <https://doi.org/10.13039/501100011033> and by the European Union NextGenerationEU/PRTR, the Fundación Ramón Areces project CIVP20A6621 and the Catalan government grant SGR221-1333.

## Author contributions

C.W. and L.Y. designed the research. W.Q. wrote the first draft of the manuscript and performed the ground-level and satellite-level analyses. H.H. conducted GUD model simulations and improvements. T.Y. and J.W. simulated and provided PM<sub>2.5</sub> data. C.M.Z. and J.P. contributed to the writing of the manuscript.

## Competing interests

The authors declare no competing interests.

## Additional information

**Supplementary information** The online version contains supplementary material available at <https://doi.org/10.1038/s41467-025-58710-9>.

**Correspondence** and requests for materials should be addressed to Le Yu or Chaoyang Wu.

**Peer review information** *Nature Communications* thanks Hyun Seok Kim, and the other, anonymous, reviewer(s) for their contribution to the peer review of this work. A peer review file is available.

**Reprints and permissions information** is available at <http://www.nature.com/reprints>

**Publisher's note** Springer Nature remains neutral with regard to jurisdictional claims in published maps and institutional affiliations.

**Open Access** This article is licensed under a Creative Commons Attribution-NonCommercial-NoDerivatives 4.0 International License, which permits any non-commercial use, sharing, distribution and reproduction in any medium or format, as long as you give appropriate credit to the original author(s) and the source, provide a link to the Creative Commons licence, and indicate if you modified the licensed material. You do not have permission under this licence to share adapted material derived from this article or parts of it. The images or other third party material in this article are included in the article's Creative Commons licence, unless indicated otherwise in a credit line to the material. If material is not included in the article's Creative Commons licence and your intended use is not permitted by statutory regulation or exceeds the permitted use, you will need to obtain permission directly from the copyright holder. To view a copy of this licence, visit <http://creativecommons.org/licenses/by-nc-nd/4.0/>.

© The Author(s) 2025